Research report

Splitting of the P3 component during dual-task processing in a patient with posterior callosal section

Guido Hesselmann [a,*], *Lionel Naccache* [b,c,d,e], *Laurent Cohen* [c,d,e] *and Stanislas Dehaene* [f,g,h]

[a] *Visual Perception Laboratory, Department of Psychiatry, Charité Campus Mitte, Berlin, Germany*
[b] *AP-HP, Groupe Hospitalier Pitié-Salpêtrière, Department of Neurophysiology, Paris, France*
[c] *AP-HP, Groupe Hospitalier Pitié-Salpêtrière, Department of Neurology, Paris, France*
[d] *INSERM, ICM Research Center, UMRS 975, Paris, France*
[e] *Université Paris 6, Faculté de Médecine Pitié-Salpêtrière, Paris, France*
[f] *INSERM, Cognitive Neuroimaging Unit, Gif sur Yvette, France*
[g] *CEA, I2BM, NeuroSpin Center, Gif sur Yvette, France*
[h] *Collège de France, Paris, France*

ARTICLE INFO

ABSTRACT

When two concurrent sensorimotor tasks have to be performed at a short time interval, the second response is generally delayed at a central decision stage. However, in patients who have undergone full or partial transection of forebrain fibers connecting the two hemispheres (split-brain), independent structures subserving all processing stages should reside in each disconnected hemisphere, thus predicting parallel processing of dual tasks. Surprisingly, this prediction is usually not verified behaviorally. We reasoned that brain imaging with high-density recordings of event-related potentials (ERPs) could clarify the extent and limits of parallel processing in callosal patients. We studied a patient (AC) with posterior callosal section in a lateralized number-comparison task. Behaviorally, the split-brain patient showed robust dual-task interference, superficially similar to the psychological refractory period (PRP) effect in the control group of 14 healthy subjects, but significantly different in important aspects such as slowing of response times in the first task. Analysis of ERPs revealed that the parietal P3 component became split into distinct contralateral components in the patient, and was dramatically reduced for targets in his left visual field. In contrast to the control group, P3 latencies showed minimal to nonexistent postponement related to dual-task processing in the patient. In summary, our findings suggest that the left and right hemisphere networks normally involved in a single distributed "global neuronal workspace" that underlies the generation of the P3 component and serial processing, became strongly decoupled after a posterior callosal lesion.

* *Corresponding author.* Department of Psychiatry, Charité Campus Mitte, 10117 Berlin, Germany.
E-mail address: g.hesselmann@gmail.com (G. Hesselmann).

1. Introduction

1.1. Dual-task performance in "split-brain" patients

Even simple "multi-tasking" situations can reveal striking capacity limits of human information processing (Marois and Ivanoff, 2005). When neurologically normal subjects are asked to perform two tasks simultaneously or in close succession, severe interference is typically observed, although performance may improve when the task-relevant items are submitted to the relatively independent processing resources of the cerebral hemispheres (Scalf et al., 2007; Banich, 1998). Here, we address the issue of how patients with disconnected hemispheres perform in such situations. A wealth of split-brain studies suggests that separate and independent structures subserving all processing stages necessary for the completion of simple sensorimotor tasks should reside in each disconnected hemisphere (Gazzaniga, 1995, 2005).

Although dual-task interactions had been studied in "split-brain" patients before [e.g., (Holtzman and Gazzaniga, 1982), patient VP], Pashler and colleagues were the first to employ a variant of the psychological refractory period (PRP) paradigm in a group of four such patients (JW, NG, VP, LB) who had undergone surgical transection of the corpus callosum for the control of intractable epilepsy (Pashler et al., 1994). In the classic PRP paradigm, two target stimuli (T1 and T2) are presented in brief succession, and subjects' responses (R1, R2) to both targets are recorded (Welford, 1952; Telford, 1931). Response times to the second stimulus (RT2) have been shown to exhibit a significant increase when the stimulus-onset asynchrony (SOA) between the two tasks is shortened, while response times to the first stimulus (RT1) remain largely unaffected by SOA. In the study by Pashler and colleagues, subjects were presented with a sequence of two stimuli in the left and right visual hemifield, and responded with the left hand to left-field stimuli and with the right hand to right-field stimuli (two-alternative forced-choice of vertical position). Thus, the input and output for each visual task were confined to either isolated hemisphere. The authors hypothesized that PRP effects should be eliminated in split-brain patients, under the assumption that the interference depends upon direct cortico-cortical connections between the two hemispheres. Surprisingly, however, patients with commissurotomy showed a strong dual-task slowing (PRP effect), which — superficially at least — seemed highly similar to that of the normal control group.

1.2. The PRP

Modern theories of the PRP, such as the central bottleneck model, commonly involve three stages of processing: a perceptual (P), a central (C), and a motor (M) stage (Pashler, 1994, 1998). According to the model, P and M stages can occur in parallel and may overlap for two tasks, while the C stage is strictly serial. Thus, at short SOAs, central processing for T2 is deferred until central processing for T1 is completed, and RT2 is increased [e.g., (Sigman and Dehaene, 2005), Fig. 1]. It has been proposed that response selection, i.e., the mapping between sensory information and motor action, forms
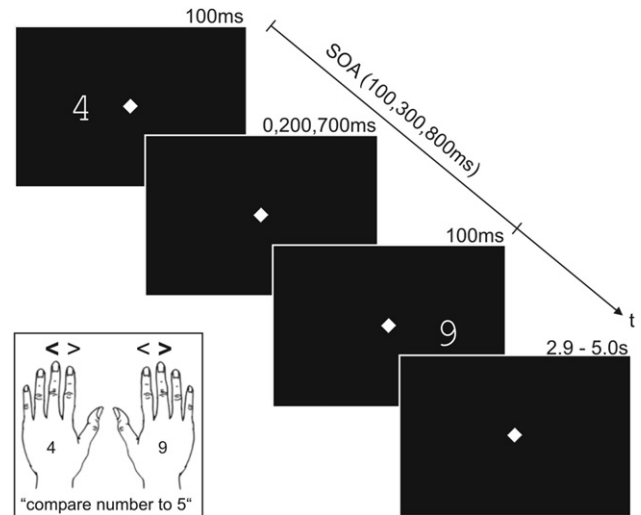

Fig. 1 — PRP paradigm. In dual-task trials, two target numbers (here, 4 and 9) were presented on the screen for 100 msec, and subjects were instructed to perform two successive number-comparison tasks ("smaller or larger than 5?"). The SOA between the first (T1) and the second target (T2) was varied between 100, 300, and 800 msec. Subjects responded to both targets with manual button presses. In two blocks of the dual-task condition, T1 was either presented on the left and T2 on the right (T1LT2R trials), or T1 was presented on the right and T2 on the left (T1RT2L). In the single-task condition, only T1 was presented, in two blocks with T1 either left (T1L) or right of fixation (T1R).

a structural bottleneck and underlies serial processing at the C stage (Pashler and Johnston, 1989; De Jong, 1993). Pashler and colleagues discussed their findings from split-brain patients within the framework of the bottleneck model, concluding that intact subcortical structures might participate in scheduling multiple stimulus-response sequences in callosum-sectioned patients. The exact nature of this coordination, however, remained to be elucidated (Pashler et al., 1994).

In a related study on motor control, it was shown that a split-brain patient (JW) could plan and produce incompatible bimanual movements without dual-task interference, thus arguing against the claim of an intact unitary response selection bottleneck in callosotomy patients (Franz et al., 1996). In a series of single-case studies on the same patient, Ivry and colleagues examined this apparent contradiction using variations of the PRP task (Ivry et al., 1998; Ivry and Hazeltine, 2000). Their results showed robust dual-task slowing in the split-brain patient, as well as in a group of control participants. Yet, the data also revealed significant differences between the patient's and the normal group's dual-task performance under different stimulus-response mappings, indicating that the dual-task slowing in callosal patients can be accounted for by a bottleneck associated with response initiation rather than response selection (Ivry et al., 1998).

A recent study argues that the apparent PRP effects in split-brain individuals are the consequences of a prioritization strategy adopted by the subjects when performing the two

tasks (Hazeltine et al., 2008). In a standard PRP experiment, although the experimenter intends the subject to respond as fast as possible to each target, the task structure and instructions might be interpreted by subjects as a need to always respond first to the first target, and second to the second one. Performing such a serial task might then be disproportionately difficult in callosal patients whose two hemispheres cannot readily exchange information about which stimulus came first. It would thus result in a conservative strategy which could severely slow down both responses. Indeed, it has been shown in normal subjects that dual-task interference can be strongly modulated by instructions about task priorities (Schumacher et al., 2001). In their study, Hazeltine and colleagues tested two split-brain patients (JW, VP) in a dual-task paradigm in which lateralized stimuli for the two tasks were presented simultaneously, and patients were instructed to simply respond to the stimuli as quickly as possible. In disagreement with previous studies (Pashler et al., 1994; Ivry and Hazeltine, 2000; Ivry et al., 1998), patients showed much smaller or nonexistent dual-task costs, which suggests that they were able to simultaneously select responses for the two hands without central processing limitations.

1.3. Event-related potential (ERP) studies of the PRP

All of the above dual-task studies relied on behavioral measures. To further explore the issue of dual-task processing with partially disconnected hemispheres, we sought to describe the neural substrates of dual-task costs and inter-hemispheric interference in a partial split-brain patient. To that aim, we recorded high-density electroencephalography (EEG) data in a patient (AC) with posterior callosal section in a lateralized PRP task. Behavioral and EEG data from our previous work on the same task (Hesselmann et al., 2011) served as healthy control group data. Our study of ERPs focused on the sensory N1 and the post-sensory P3 components, using a linear regression method optimally suited for the analysis of single-trial data.

A number of previous ERP studies investigating the PRP effect have targeted the amplitude and latency of the P3(b) component, which is characterized by a positive deflection broadly distributed over the scalp, with a focus over parietal electrodes (Picton, 1992). The P3 has been associated with post-perceptual processes such as the context-updating of working memory (Donchin and Coles, 1988; Donchin, 1981), decision-related processing (Verleger et al., 2005), and the access of a target stimulus to a global neuronal workspace necessary for conscious report (Sergent et al., 2005; Del Cul et al., 2007). Previous dual-task investigations have provided evidence for a sensitivity of P3 amplitude to dual-task interference (Isreal et al., 1980; Kok, 2001). Based on the observation that P3 latencies showed significant postponement directly proportional to the PRP effect, some studies have proposed that the P3(b) component primarily indexes the central cognitive processes mediating the PRP effect (Dell'Acqua et al., 2005; Sigman and Dehaene, 2008; Hesselmann et al., 2011). Evidence from other studies, however, occasionally shows large discrepancy between RT2 and T2-P3 latency modulations, suggesting at least partially independent sources for PRP and P3

effects (Luck, 1998; Arnell et al., 2004). The latencies of earlier sensory ERP components, such as the P1 and N1, have been consistently reported to remain stimulus-locked to both targets and show no postponement related to the PRP (Brisson and Jolicœur, 2007; Sigman and Dehaene, 2008).

In this context, the main question of our study was whether the P3 responses would show a PRP delay in a callosal patient, in a paradigm that systematically reveals such a delay in normal subjects (Hesselmann et al., 2011). Based on the previously mentioned behavioral study by Hazeltine et al. (2008), we predicted that the P3 wave might indicate a great degree of parallel processing in our partial split-brain patient, even if the behavioral responses superficially suggest a dual-task delay.

2. Materials and methods

2.1. Participants

The patient (AC) tested in this study was a 36-year-old male right-handed native French speaker. He obtained the baccalauréat (French high school graduation) and completed two years of university studies. Following surgery for a cerebral hemorrhage in his left mesial parietal lobe due to a small arteriovenous malformation, he presented a partial section of the posterior half of the corpus callosum [for more details and anatomical images, see (Intriligator et al., 2000; Cohen et al., 2000)]. A magnetic resonance imaging (MRI) examination revealed a porencephalic cyst in the left parietal lobe (Frak et al., 2006) and a cut of the posterior half of the corpus callosum (Michel et al., 1996), from the posterior midbody (III) to the splenium (V), according to the tractography-based parcellation by Hofer and Frahm (2006). At the time of the study in April 2008, approximately 14 years after surgery, AC worked as an accountant, had normal visual fields, no signs of optic ataxia, no paresis or hypesthesia, no simultanagnosia or visual neglect, and no apraxia. The experiment was conducted at the Department of Neurology at the Pitié-Salpêtrière hospital in Paris, France. The healthy sample consisted of 14 male right-handed native French speakers who participated in a previously published EEG-functional MRI (fMRI) experiment (Hesselmann et al., 2011), which was conducted at the NeuroSpin neuroimaging center in the CEA campus of Saclay, France. Behavioral data from this study were re-analyzed in the current study. To increase statistical power, we included behavioral data from two subjects which had been excluded previously based on neuroimaging data. All healthy subjects (mean age 23, range 19—28 years) had normal or corrected-to-normal vision. All participants provided informed written consent to take part in the experiment.

2.2. Design and procedure

The experimental design was identical to that from our previous study (Hesselmann et al., 2011). The patient and the control subjects were asked to perform two number-comparison tasks ("smaller or larger than 5?") on two successive digits presented left or right of fixation. Smaller-larger magnitude comparison has previously been shown to be

spared for left visual field (LVF) and right visual field (RVF) targets in split-brain patients (Colvin et al., 2005; Seymour et al., 1994) as well as in a patient with posterior callosal lesion (Cohen and Dehaene, 1996), when quantities are represented in form of Arabic digits. All subjects were instructed that they had to respond accurately and as fast as possible to each of them, according to the order of their appearance. The target stimuli (numbers 1, 4, 6, or 9) were presented in white font ("Courier New") on a black background for 100 msec (Fig. 1) using Eprime software (Version 1.1, Psychology Software Tools Inc., USA). The SOA between the first (T1) and the second target (T2) was varied between 100, 300, and 800 msec. The size and eccentricity of the target stimuli were carefully chosen so that subjects could perform the number-comparison task while maintaining fixation; we observed only small (<2 μV) and infrequent eye movements in the patient, both in the single-task and in the dual-task conditions (Supplementary Fig. 1). Target stimuli covered $1.7 \times 2.9°$, and were presented either $3.0°$ left or right of a diamond-shaped fixation point ($.5°$). Subjects responded to both targets with button presses, with the left hand to LVF targets, and with the right hand to RVF targets. For left targets, the middle finger served for responses to numbers smaller than 5, the index finger for numbers larger than 5; for right targets, the index finger served for responses to numbers smaller than 5, the middle finger for numbers larger than 5. No error feedback was given.

In the dual-task condition, all subjects performed blocks of 144 trials (48 trials per SOA). Care was taken that all possible combinations of target numbers (T1, T2) were approximately balanced for each SOA (quasi-randomization). In one block, T1 was presented on the left and T2 on the right (T1LT2R). In another block, T1 was presented on the right and T2 on the left (T1RT2L). In the single-task condition, only T1 was presented, in blocks of 48 trials with T1 either left (T1L) or right of fixation (T1R). The length of each trial was jittered between 3.8 and 5.2 sec in .2 sec steps (mean: 4.5 sec), and subjects could respond within that period. The order of trials in each block, as well as the order of blocks was randomized. Patient AC performed each type of experimental block twice during EEG recordings, healthy subjects performed all blocks once during simultaneous EEG-fMRI measurements. Before the main experiment, all subjects were extensively trained on the task (25 min).

2.3. Behavioral data analysis

Response times to the first (RT1) and second target (RT2) were determined separately for each subject and condition. Dual-task trials were divided into congruent (both target numbers smaller or larger than 5) and incongruent trials. Trials with RT1 or RT2 outliers (i.e., response times shorter than the first quartile minus 1.5 times the inter-quartile range, or longer than the third quartile plus 1.5 times the inter-quartile range) were excluded from all further analysis. Separately for the first (R1) and second responses (R2), response times were submitted to repeated-measures analysis of variance (ANOVA) with single-trials as the replication factor using SPSS 13.0 for Windows (SPSS Inc., USA). In all ANOVAs (including behavioral and EEG data), the Greeenhouse—Geisser correction (ε) was applied to account for possible violations of sphericity (Greenhouse and Geisser, 1959). The uncorrected

degrees of freedom are reported. Note that there are no random subject effects in this single-case study and our inference pertains to this and only this subject (as opposed to the population of subjects from which our subject was drawn). This is why the ANOVA's degrees of freedom reflect the number of samples, as opposed to the number of subjects. We report partial eta squared (η^2) as an estimation of effect size. As a rough guideline, eta squared of .01 constitutes a small effect, .06 a medium effect and .14 a large effect (Cohen, 1988). To test for differences between patient AC's task performance and performance in the healthy subjects, we used a t-test specifically developed for single-case studies (Crawford and Howell, 1998). This modified t-statistic tests for the rarity or abnormality of a patient's score, using the standard deviation (SD) of a group of healthy subjects (as the normative sample of size N) as an estimate for the population SD and N-1 degrees of freedom. Pearson's correlation coefficients were Fisher z-transformed for all statistical analyses.

2.4. EEG acquisition and preprocessing

In patient AC, continuous EEG was acquired from 256 channels using a NetAmps-300 amplifier and a HydroCel Geodesic Sensor Net with Ag/AgCl electrodes (EGI, USA) referenced to the vertex. The resolution and dynamic range of the EEG amplifier were .07 μV per bit and ±200 mV, respectively. EEG was sampled at 250 Hz and bandpass-filtered online between .1 and 100 Hz. Using the EGI Waveform Tools, epochs with voltages exceeding ±125 μV and transients exceeding ±100 μV were rejected, the EEG data were bandpass-filtered offline (.5—40 Hz), epoched ($-.2$—1.6 sec, time-locked to T1 onset), re-referenced to average reference, and exported to EEGLAB 6.03b (Delorme and Makeig, 2004) running on Matlab 7.1R14 (The Mathworks, USA) for all further preprocessing and analysis. After dimensionality reduction to 64 dimensions based on principle component analysis (PCA), independent-component analysis (ICA) was performed on the concatenated single-trial EEG data, separately for single-task, T1LT2R and T1RT2L experimental blocks, using the extended INFOMAX algorithm as implemented in EEGLAB (Bell and Sejnowski, 1995). The resulting 64 independent components (ICs) were automatically classified using the ADJUST toolbox (Mognon et al., 2011) and rejected if classified as artifact (i.e., eye blink, eye movement, and generic discontinuity). Eight ICs were rejected in the single-task trials, 13 in the T1LT2R trials, and four in the T1RT2L trials. In healthy subjects, continuous EEG was acquired from 64 channels during simultaneous EEG-fMRI recordings [for details, see (Hesselmann et al., 2011)]. All topographical maps were created using the open-source toolbox Fieldtrip (Oostenveld et al., 2011).

2.5. EEG analysis

To understand the dynamics of the different brain processes involved in the dual-task condition and to allow statistical testing of our single-case data, we sought to decompose the EEG data into ERP components of interest, on a trial-by-trial basis. To achieve this aim, we applied a linear regression method used in previous EEG studies of the PRP (Sigman and Dehaene, 2008; Hesselmann et al., 2011; Marti et al., 2012). In

brief, multi-channel time-series of EEG data ("spatio-temporal templates") for each ERP component of interest (N1, P3) were extracted from the single-task condition in which these components did not overlap. Multiple linear regression was then used to project, for each time point, the EEG to the previously defined component templates. The resulting time-series of parameter estimates (beta values) quantify, for each time point, to what extent ERP component activity comparable to the single-task condition was present in the dual-task condition. Note that the regression method provides powerful denoising of the EEG signal thus making it well suited for the statistical analysis of single-trial data in our single-case study. The following paragraphs provide a more detailed description of the method.

First, we defined spatio-temporal templates which were designed to capture the temporal and scalp distribution characteristics of the N1 and P3. Two templates were used for the components evoked by left and right single targets (T1L and T1R), respectively. Estimation of the onsets of the N1 and P3 components was based on the time course of the global field power (GFP) (Lehmann and Skrandies, 1980). As can be seen in Fig. 4A, a first GFP maximum occurred at approximately 168 msec, and a second GFP maximum started at

approximately 328 msec. The corresponding ERP topographies at 168 msec revealed the posterior negativity of the lateralised T1L-N1 and T1R-N1 components (Fig. 4B). The ERP topography at 328 msec revealed the parietal positivity of the T1L-P3 and T1R-P3. In contrast to the data from the healthy subjects, the P3 components appeared to be as lateralised as the N1 components. The smaller peak at 112 msec corresponded to the sensory P1 component which was not analyzed further. Intermediate and later GFP peaks could not be associated with known ERP components. The spatio-temporal distributions were extracted from the EEG data based on the corresponding peaks, as follows: for the N1, we used the voltages in a 100 msec window centered on 168 msec after the single target onset, thus from 118 to 218 msec; similarly, for the P3, we used the voltages in a 200 msec window centered on 328 msec (i.e., from 228 to 428 msec after single target onset), thus non-overlapping with the N1 time window. Note that we chose a longer template for the P3 to account for the broader maximum of this component.

Next, for each time point of the EEG, we used a multiple linear regression procedure on sliding windows of data to extract the single-trial temporal profiles of the four spatio-temporal components (LVF-N1, RVF-N1, LVF-P3, RVF-P3).
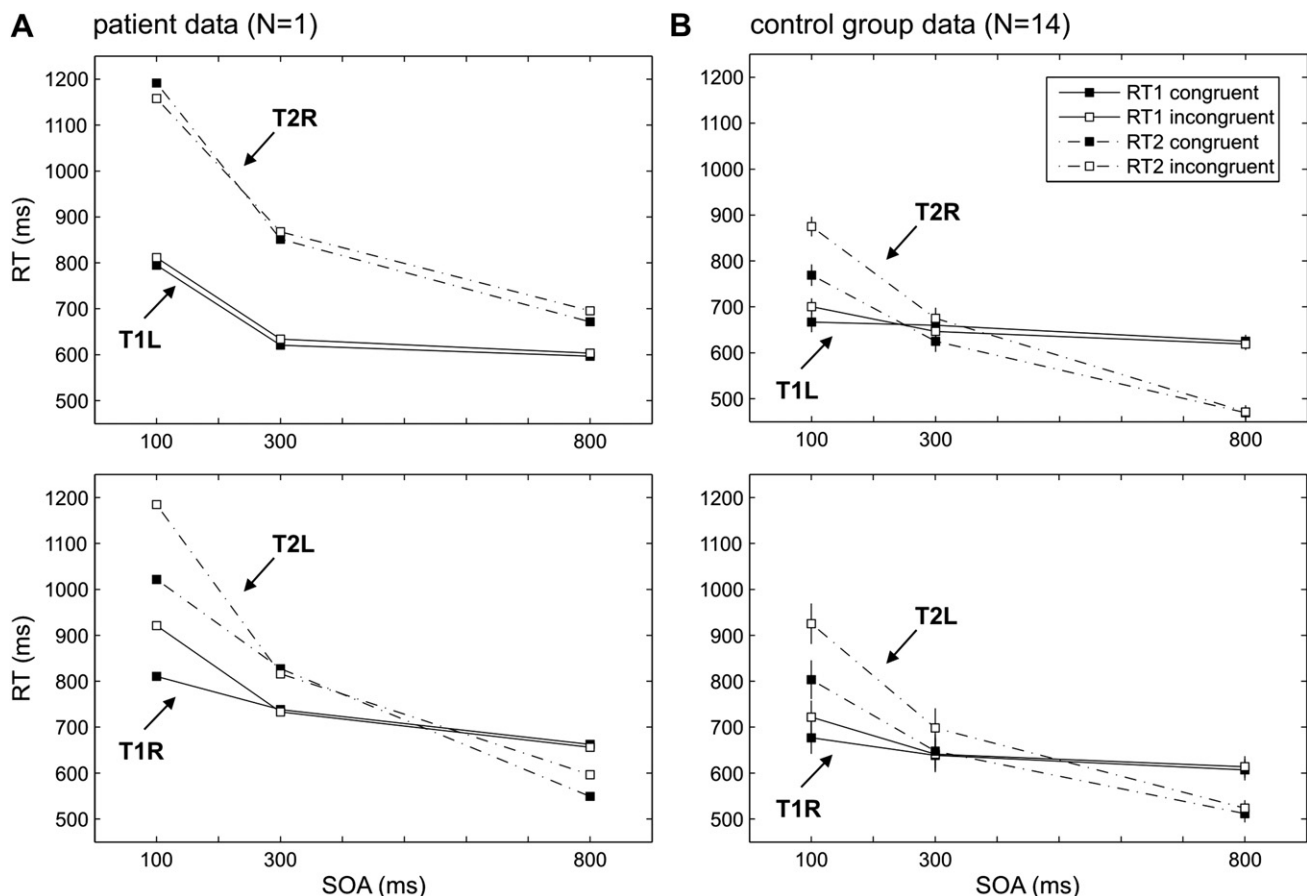

Fig. 2 – Behavioral PRP results. Average RTs at SOAs 100, 300, and 800 msec are shown for responses to the first target (RT1, solid lines) and to the second target (RT2, dashed lines), separately for congruent and incongruent trials (filled and open squares, respectively). (A) Split-brain patient data (N = 1). (B) Data from the healthy control group (N = 14). Error bars represent standard error of the mean (±SEM). Upper and lower panels show data from T1LT2R and T1RT2L trials, respectively.

High beta weights, for a given time point, indicate a good fit between the EEG data and the spatio-temporal template within the corresponding time window. Single-trial beta weights are presented as "ERP-images", as provided by the EEGLAB software (Figs. 4D, 7 and 8). These plots are color-coded (red: positive values, green: zero, blue: negative). For better visualization, single-trial beta weights were smoothed across trials with a 20-trials wide moving rectangular window.

Finally, the extracted single-trial beta weights were submitted to statistical analysis. To test for significant deviations from zero, beta weights in all dual-task conditions were submitted to one-sample, one-tailed permutation t-tests with correction for multiple comparisons (Blair and Karniski, 1993), using the Mass Univariate ERP Toolbox developed at the Department of Cognitive Science at the University of California, San Diego (Groppe et al., 2011).We used 5000 permutations to estimate the distribution of the null hypothesis, and an alpha-level of .005 to obtain the critical t-scores (tmax). In Figs. 3, 4C, 7 and 8, gray horizontal bars above the x-axis indicate significant time points; points within a consecutive series of at least 10 significant time points (40 msec) are color-coded according to condition. To test for differences between beta weights in different conditions, we extracted single-trial beta weights for time windows centered on the average peaks of the corresponding components. N1 betas were extracted over a time window of ±24 msec around the peak time; P3 betas were extracted over a time window of ±48 msec around the peak time. In this way, we obtained, for each trial and each condition, a beta value for N1 and P3. The single-trial beta values were submitted to repeated-measures ANOVA with factors "SOA" and "hemisphere". Analysis of beta weights using non-parametric randomization tests (Todman and Dugard, 2001) instead of repeated-measures ANOVA yielded the same statistical results as reported in our paper.

3. Results

3.1. Behavioral results: PRP effect

Table 1 provides a summary of patient AC's response accuracies and reaction times (RTs). In single-task trials, patient AC's response accuracy rates were comparable to those observed in the healthy sample [94.3% vs 96.3 $\pm$ 2.67%; mean $\pm$ SD; $t_{13} < 1$]. In dual-task trials, they were slightly but significantly lower than in the healthy group (86.0% vs 94.4 $\pm$ 3.21%; $t_{13} = 2.53$, $p = .013$), and comparable for the first (87.7%) and second responses (84.4%). The patient's response accuracies were only minimally modulated by SOA and by the laterality of target stimuli. Error trials were removed from all further analyses (behavioral, EEG).

In the single-task condition, the patient's mean RT was significantly shorter for LVF targets (T1L: 516 $\pm$ 67 msec; mean $\pm$ SD) than for RVF targets (T1R: 653 $\pm$ 157 msec; $F_{1,86} = 59.23$, $p < .001$, $\eta^2 = .41$). As can be seen in Fig. 2A, a similar effect of visual field was observed in dual-task trials: RT1 was 677 $\pm$ 146 msec for LVF targets in T1LT2R trials and 756 $\pm$ 239 msec for RVF targets in T1RT2L trials ($F_{1,217} = 18.73$, $p < .001$, $\eta^2 = .079$); RT2 was 833 $\pm$ 216 msec for LVF targets in T1RT2L trials and 906 $\pm$ 215 msec for RVF targets in T1LT2R
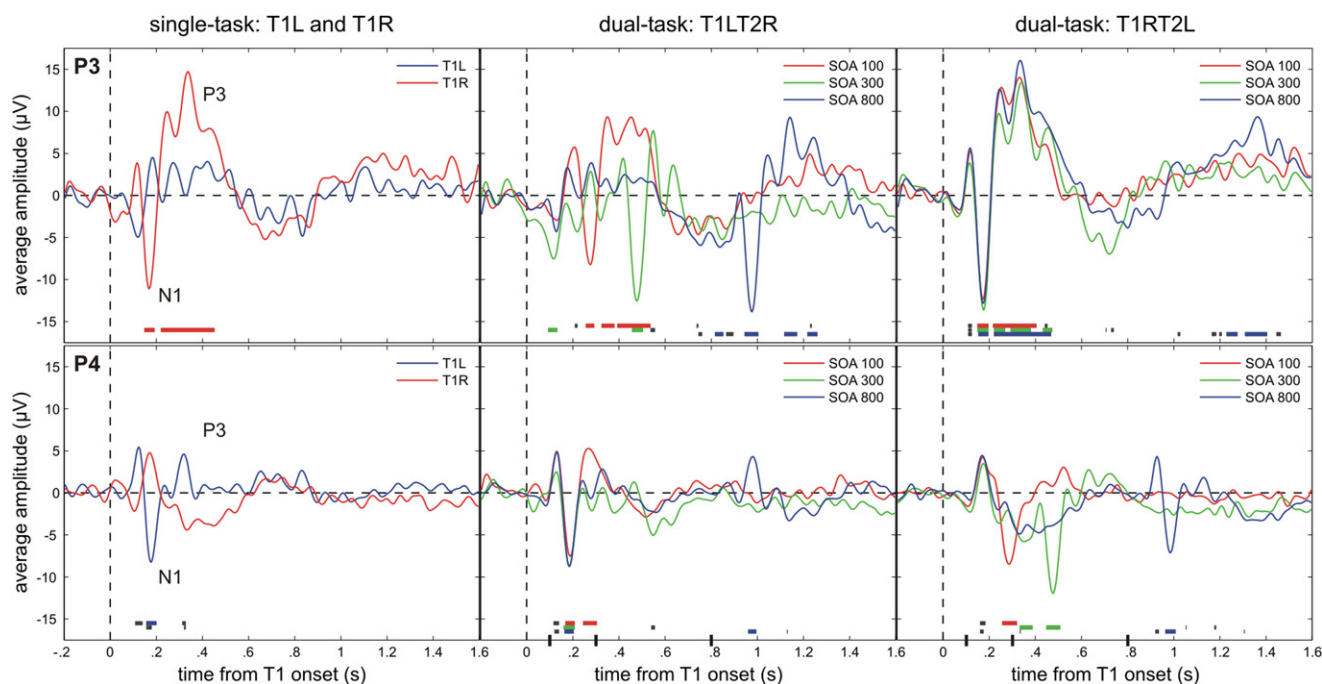

Fig. 3 − Average patient ERPs relative to T1 onset at parietal electrodes P3 and P4, in single-task trials (left panels), dual-task T1LT2R trials (middle panels), and dual-task T1RL2L trials (right panels). Gray horizontal bars indicate significant time points; significant time points within a consecutive series of at least 10 significant time points (40 msec) are color-coded according to condition. Small vertical bars on the x-axis indicate T2 onset at SOA 100, 300, and 800 msec in dual-task trials. For display purposes, the ERP data have been subjected to a 20 Hz low-pass filter.
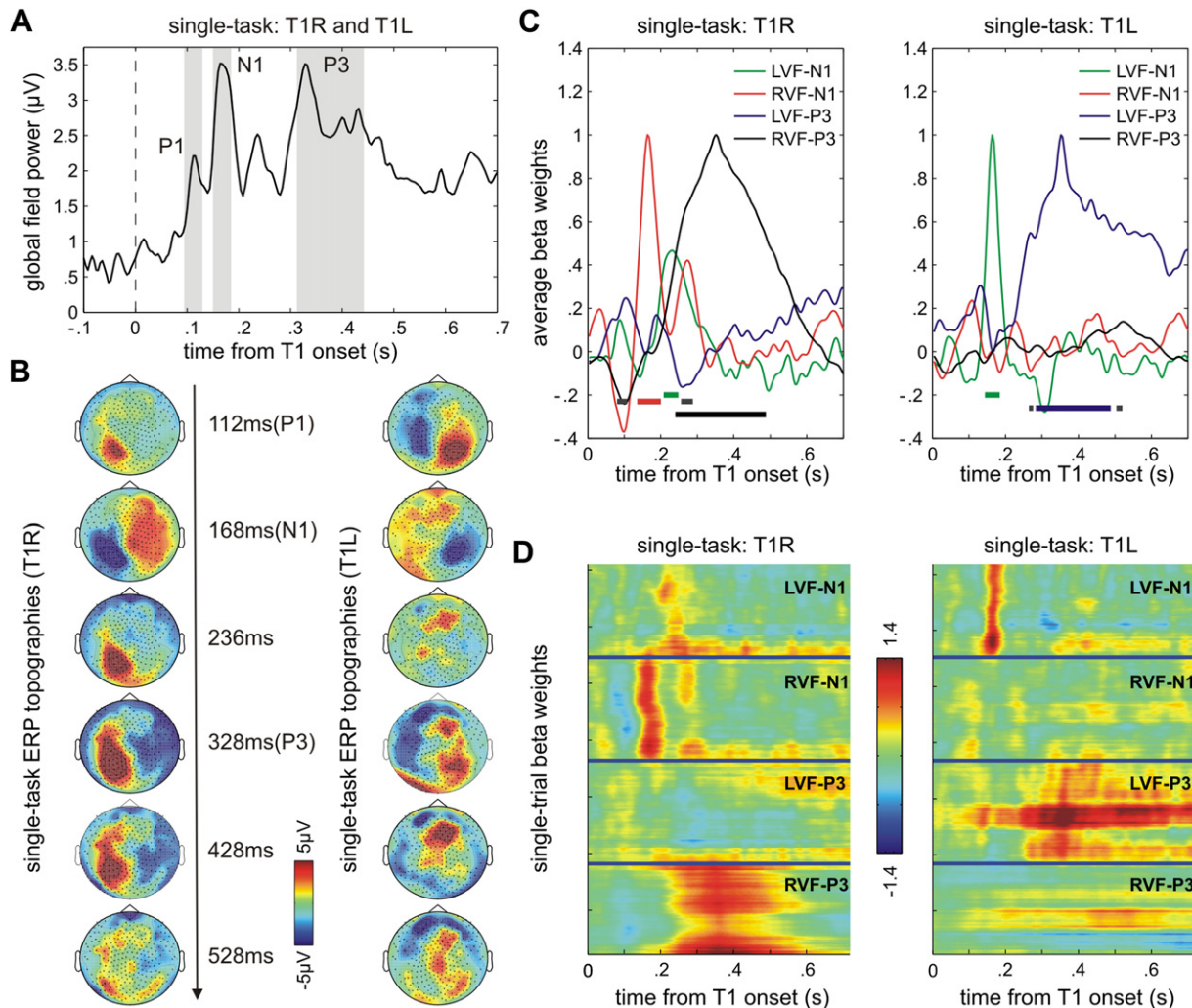
Fig. 4 — Analysis of ERPs in single-task trials. (A) Average GFP of ERPs in T1R and T1L trials. GFP peaks were used to identify ERP components P1, N1, and P3 (gray rectangles). Intermediate and later peaks could not be associated with known ERP components. The black rectangle on the x-axis represents the on- and offset of the stimulus. (B) The 2D scalp topographies show the ERP topographies evoked by right targets (T1R) and left targets (T1L) at six different time points (112 = P1, 168 = N1, 236, 328 = P3, 428, and 528 msec). Small circles represent single electrodes; Pz is the fifth midline channel from the bottom. (C) Results of the multiple regression method applied to single-task trials. Beta weights for T1-N1 (green, red) and T1-P3 (blue, black) are plotted against time from T1 onset. Horizontal bars above the x-axis indicate significant time points (deviation from zero). (D) Plot of single-trial beta weights in T1R and T1L trials, color-coded (red: positive, green: zero, blue: negative). Ticks on the y-axis are every 50 trials.

trials ($F_{1,217} = 4.20$, $p = .042$, $\eta^2 = .02$). In healthy subjects, visual field did not modulate RT (Fig. 2B). Overall RTs in single-task trials (534 ± 20 msec; mean $\pm$ SE), and RT1 in dual-task trials (651 ± 22 msec) were comparable to the patient's performance ($t_{13} < 1$), while RT2 was significantly shorter in the control group (666 ± 24 msec; $t_{13} = 2.19$, $p = .024$).

Fig. 2A illustrates that, in both trial types, the patient's RT2 increased significantly with decreasing SOA, in accordance with the classical PRP model (Pashler, 1994; Pashler and Johnston, 1989). RT1 showed a smaller, yet consistent and significant increase with decreasing SOA. In T1LT2R trials, RT2 increased by 491 msec as SOA decreased from 800 to 100 msec, while RT1 increased by 203 msec over the same time range.

In T1RT2L trials, the corresponding values were 531 msec and 205 msec. The F ratios and partial eta squared values underline the difference in magnitude between the main effects of SOA for RT1 and RT2, both in T1LT2R trials (RT1: $F_{2,66} = 29.95$, $p < .001$, $\eta^2 = .48$, $\varepsilon = .66$; RT2: $F_{2,66} = 91.89$, $p < .001$, $\eta^2 = .74$, $\varepsilon = .84$) and in T1RT2L trials (RT1: $F_{2,72} = 13.68$, $p < .001$, $\eta^2 = .28$, $\varepsilon = .96$; RT2: $F_{2,72} = 107.77$, $p < .001$, $\eta^2 = .75$, $\varepsilon = .74$).

Taking only RTs at SOAs 100 and 300 into account (i.e., SOAs within the interference regime), the RT2 slopes were -1.56 for T1LT2R trials and -1.41 for T1RT2L trials, thus larger than the theoretical slope of -1 predicted by the classical PRP model for short SOAs. In the healthy sample, the corresponding RT2 slopes were $-.86 \pm .06$ (mean $\pm$ SE) and $-.96 \pm .07$, respectively
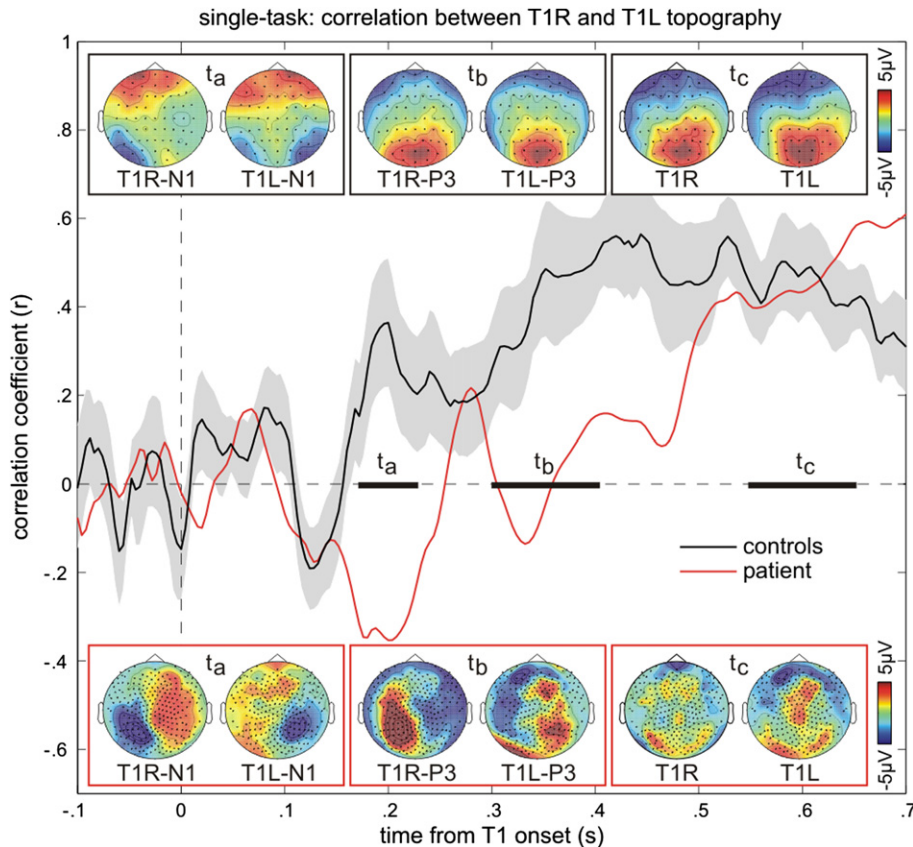
Fig. 5 — Correlation between T1R and T1L single-task ERP topographies. The solid lines represent the moment-to-moment Pearson correlation coefficients (r) between ERP topographies evoked by T1R and T1L targets in single-task trials (red: patient data, N = 1; black: healthy control group data, N = 12). Separately for the controls (upper panels) and the patient (lower panels), topographies in T1R and T1L trials are shown for time points t_a (controls: 200 msec, patient: 168 msec), t_b (controls: 380 msec, patient: 328 msec), and t_c (controls: 580 msec, patient: 580 msec). The topographies are 2D representations of the different 3D electrode layouts (patient: 256 electrodes, Pz is the fifth midline channel from the bottom; controls: 62 electrodes, Pz is the third midline channel from the bottom). To reduce noise in the patient data, the correlation values were smoothed with a moving average filter (length: 15 data points, 60 msec). The gray shading represents ±SEM.

(Fig. 2B). The test for a difference in RT2 slopes between the patient and the healthy sample yielded significant results for both trial types (T1LT2R: $t_{13} = 3.04$, $p = .005$; T1RT2L: $t_{13} = 1.77$, $p = .049$). In T1LT2R trials, RT1 slopes at short SOAs were significantly larger for the patient than in the healthy sample ($-.88$ vs $-.15 \pm .05$, $t_{13} = 3.82$, $p = .001$), but not in T1RT2L trials ($-.61$ vs $-.30 \pm .06$, $t_{13} = 1.28$, $p = .112$).

In a next step, we analyzed RT1-RT2 correlations across SOAs. If central T2 processing is indeed postponed by central processing of T1, then RT1 and RT2 should be more strongly correlated at shorter SOAs, since the slowing in the first task is propagated onto the second task (Pashler, 1994). In T1LT2R trials, the Pearson correlation coefficient for patient AC dropped from .76 at SOA 100 and .31 at SOA 300 to .01 at SOA 800; in T1RT2L trials, the coefficients were .80, .81, and .26, respectively (Supplementary Fig. 2). Overall, there appeared to be a good correspondence between RT1-RT2 correlations in patient AC and in the healthy sample; t-tests for all SOAs yielded no consistent differences between correlation coefficients in T1LT2R trials ($t_{13} = .52$, $p = .306$; $t_{13} = 2.23$, $p = .022$; $t_{13} = 1.20$, $p = .126$), and in T1RT2L trials ($t_{13} = .39$, $p = .352$;

$t_{13} = 1.15$, $p = .135$; $t_{13} = .55$, $p = .296$; not corrected for multiple comparisons).

3.2. Behavioral results: crosstalk effects

In our dual-task paradigm, the comparison between congruent and incongruent trials allowed for the analysis of crosstalk between T1 and T2 processing. Crosstalk is defined as an effect of the congruency of the two target responses (here, both larger or both smaller than 5) on RT1 and RT2, respectively. The dependence of RT1 on the response that is required for the second stimulus is referred to as backward crosstalk (as opposed to crosstalk from T1 on RT2). Backward crosstalk effects, which are usually observed when both tasks are similar [(Logan and Delheimer, 2001; Logan and Schulkind, 2000), but see (Miller, 2006)], appear to be in disagreement with the strictly serial bottleneck model, and have been interpreted as supporting central resource sharing models (Navon and Miller, 2002; Tombu and Jolicœur, 2003) whereby the two tasks are performed partially in parallel and with continuous variable relative priorities. They remain
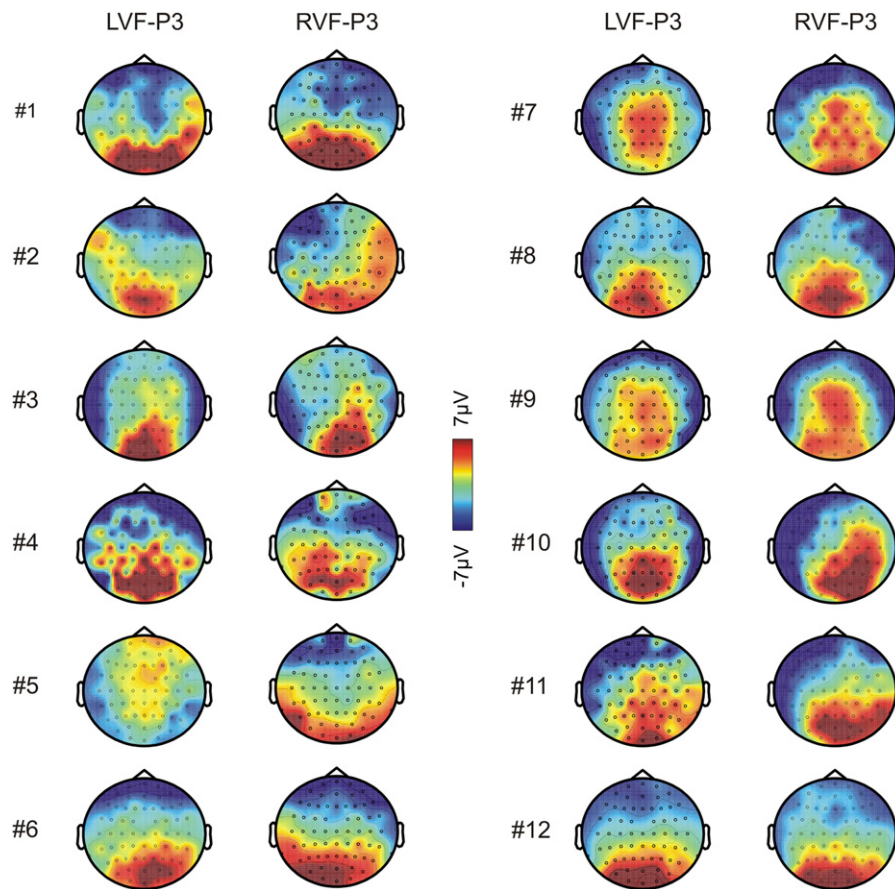
Fig. 6 – Individual P3 topographies for all EEG control subjects. Shown are the LVF-P3 (i.e., P3 evoked by targets in the LVF) and RVF-P3 at 380 msec relative to T1 onset. Note that, in control subjects, EEG data were recorded simultaneously with fMRI, and that EEG data quality is usually lower in such combined EEG-fMRI setups due to the interference between the two recording methods. The topographies are 2D representations of the 3D electrode layout (62 electrodes, Pz is the third midline channel from the bottom).

compatible, however, with strictly serial processing of the two decisions, only with a partial "leakage" of sensory evidence from one target on the decision concerning the other. The leakage account builds upon the notion that the serial processing bottleneck can be characterized as the accumulation of evidence toward a decision boundary (Sigman and Dehaene, 2005). In the current number-comparison paradigm, the possibility of leakage of evidence is made more likely by the finding that unattended and even subliminal digits can automatically access a representation of their magnitude (Naccache and Dehaene, 2001; Dehaene et al., 1998; Sackur et al., 2008).

Visual inspection of Fig. 2A reveals that crosstalk and backward crosstalk appeared to be present at SOA 100 in T1RT2L trials (lower panel), but were virtually absent in T1LT2R trials (upper panel). Based on our previous findings (Hesselmann et al., 2011), we restricted the analysis of crosstalk effects to the shortest SOA, and calculated repeated-measures ANOVAs with factors "congruency" and "T1 laterality", separately for RT1 and RT2 data. The main effect "congruency" was not significant (RT1: $F_{1,33} = 2.64$, $p = .114$, $\eta^2 = .07$; RT2: $F_{1,33} = 1.43$, $p = .241$, $\eta^2 = .04$). The "congruency × laterality" interaction turned out to be

significant for crosstalk in RT2 ($F_{1,33} = 5.37$, $p = .027$, $\eta^2 = .14$) but not for backward crosstalk in RT1 ($F_{1,33} = 1.90$, $p = .177$, $\eta^2 = .06$).Explorative analysis of backward crosstalk in T1RT2L trials revealed only a marginally significant effect ($F_{1,38} = 3.25$, $p = .079$, $\eta^2 = .08$).

Fig. 2B shows that, in the healthy sample, neither crosstalk effect was modulated by the laterality of the first target (all Fs < 1); in both trial types, crosstalk from T1 to T2 in the RT2 data was larger than backward crosstalk from T2 to T1 in the RT1 data, and crosstalk was more pronounced at the shortest SOA, as described in more detail in our previous study (Hesselmann et al., 2011). Finally, we directly compared crosstalk at SOA 100 between the patient and the healthy control group. In T1LT2R trials, crosstalk from T1 to T2 was larger in the control group ($t_{13} = -2.37$, $p = .017$), but we found no significant difference for backward crosstalk ($t_{13} = -.36$, $p = .363$). In T1RT2L trials, differences between crosstalk effects in the split-brain patient and control group were not significant ($t_{13} = 1.05$, $p = .157$; $t_{13} = 1.43$, $p = .088$).

In sum, the PRP effect was only superficially present in the callosal patient (SOA effect on RT2, RT1-RT2 correlations), but it lacked important characteristics, as attested by significant
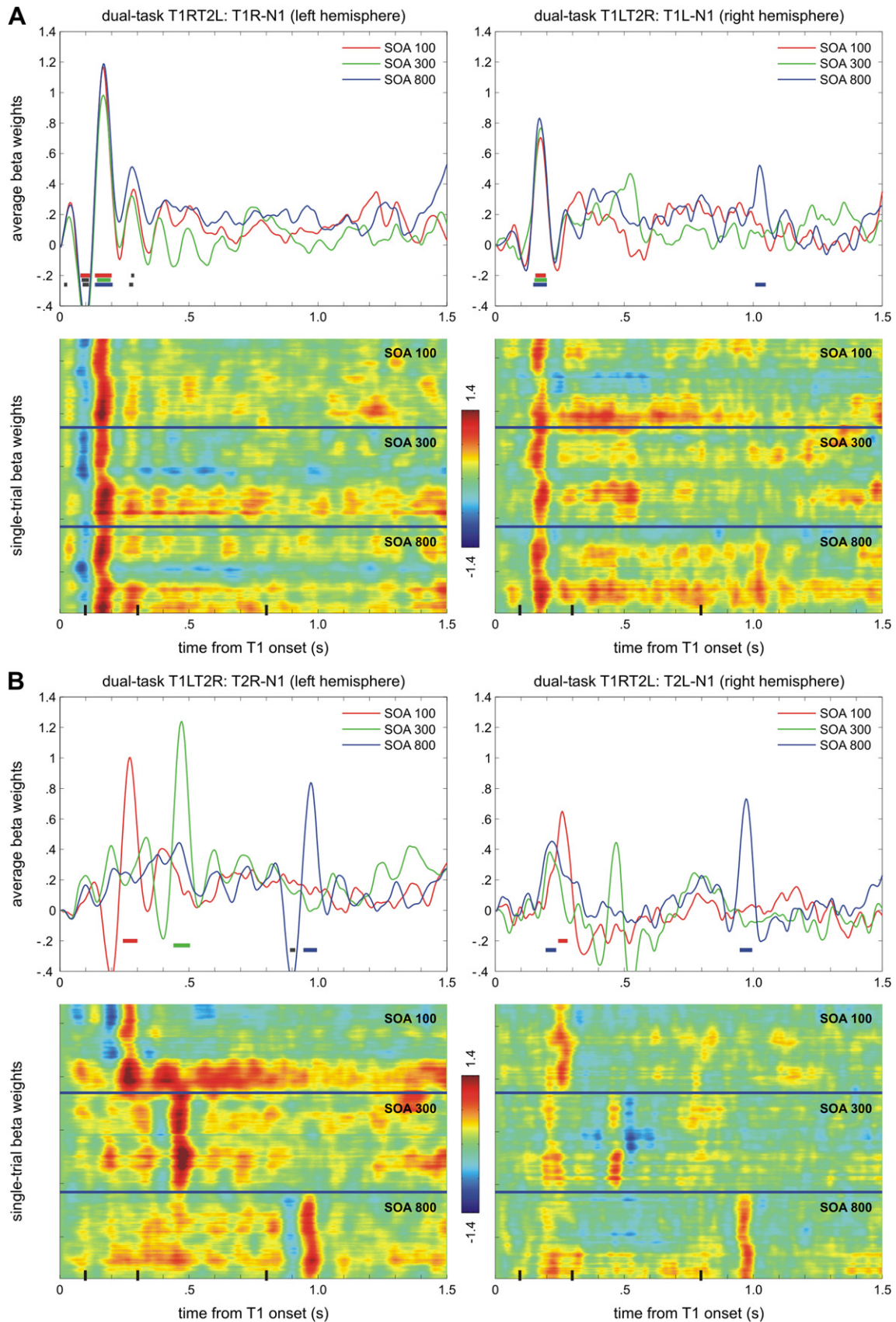
Fig. 7 – Analysis of sensory ERP components in dual-task trials. (A) T1-N1 responses. The upper panels show average beta time courses in T1RT2L and T1LT2R trials, separately for SOA 100 (red), SOA 300 (green), and SOA 800 (blue). The upper left panel shows T1-N1 activity in the left hemisphere, the upper right panel shows T1-N1 activity in the right hemisphere. In

differences between the patient's and the control group's behavioral data (SOA effect on RT1, RT slopes, crosstalk).

3.3. EEG results: ERPs in single-task and dual-task trials

Fig. 3 shows the patient's average ERPs in single-task (T1L, T1R) and dual-task (T1LT2R, T1RT2L) trials at parietal electrodes P3 and P4. As can be seen, the N1 remained stimulus-locked to the first and second target, respectively, over both hemispheres. The P3 component appeared to be much smaller at electrode P4 than at electrode P3 in single-task trials, and was virtually absent at electrode P4 in dual-task trials. Over the left hemisphere (at electrode P3), the latency of the P3 component evoked by the second target showed only small variation with SOA. These observations will be analyzed in more detail using multiple linear regression in the following sections.

3.4. EEG results: single-task (N1 and P3)

Fig. 4B illustrates that the ERP topographies evoked by targets in T1L and T1R trials revealed a strikingly long-lasting lateralization of activity. In contrast to the EEG data from the healthy subjects, where a single P3 component with broad parietal topography was evoked by both LVF and RVF targets (Hesselmann et al., 2011), even at the time of maximal P3 activity (328 msec) the topography observed in the patient appeared to be as contralateral as at the peak time of the sensory P1 (112 msec) and N1 (168 msec). To corroborate this result, Fig. 5 plots, as a function of time from T1 onset, the moment-to-moment correlation between the topographies observed in T1L and T1R trials, separately for the patient and the controls. Correlation coefficients indicate the degree of similarity between the topographies. Already at the time of the N1 component (t_a: 175−225 msec), ERPs showed evidence of inter-hemispheric transfer in normals, as attested by a positive correlation of topographies and the presence of an ipsilateral N1, as previously reported [e.g., (Johannes et al., 1995)]. By contrast, the patient's ERPs showed almost "inverse" topographies in T1L and T1R trials with a strictly contralateral N1, resulting in negative correlation coefficients in the same time range (Cohen et al., 2000). For the controls, the coefficients indicated a second convergence toward a shared topography during the time of the central P3 (t_b: 300−400 msec), which remained stable until a later time period (t_c: 550−650 msec). In the patient, however, topographies did not converge toward

a shared pattern during the time of the P3 (t_b), but only at a much later time of ~600 msec after target onset (t_c). Thus, the patient's P3 was "split" into two distinct P3's, one evoked by LVF targets, the other evoked by RVF targets. Further analysis of individual subject P3 topographies in healthy controls revealed that none of the control subjects showed a lateralization of the P3 comparable to that of the patient (Fig. 6). As a consequence of this finding, we used four spatio-temporal profiles (LVF-N1, RVF-N1, LVF-P3, RVF-P3) when applying the multiple linear regression procedure to the patient data. Note that we refer to ERP components evoked by LVF targets as LVF-N1 and LVF-P3, and to components evoked by RVF targets as RVF-N1 and RVF-P3.

Fig. 4C shows the results of the multiple regression method applied to single-target trials. Note that the definition of the component profiles was based on these data, and that we performed this analysis primarily to verify the capacity of the multiple regression method to separate neural events unfolding over time. In both T1R and T1L trials, betas for the contralateral N1 and P3 show significant peaks at the expected latencies of 168 and 328 msec, respectively. In the healthy control group, N1 and P3 beta peaks were observed at 200 and 496 msec, respectively (Hesselmann et al., 2011), but P3 related activity started already at approximately 400 msec. The time-series of beta values related to the ipsilateral N1 and P3 components, on the other hand, show no significant peaks. This finding confirms that all four ERP components could be reliably separated in the EEG data of the single-task condition.

Fig. 4D illustrates the same results as color-coded single-trial data plots, and confirms the successful separation of neural events at the single-trial level. However, there appears to be a striking difference between post-sensory processing in the left and right hemisphere. While the RVF-P3 activity in T1R trials (i.e., in the left hemisphere) is temporally well-confined and reliably detectable in almost all trials, the LVF-P3 activity in T1L trials (i.e., in the right hemisphere) appears to be much less reliable and not present in all trials. Based on this result, we re-analyzed the EEG data in order to further optimize all artifact correction methods, but the LVF-P3 beta results remained virtually the same.

3.5. EEG results: dual-task (N1)

In the next step, multiple regression analysis was used to parse the event-related neural activity in dual-task trials.

the left hemisphere, N1 can be detected at all SOAs (latency: 168 msec). In the right hemisphere, N1 appears to be smaller at all SOAs (latency: 172 msec). Horizontal bars above the x-axis indicate significant time points (deviation from zero). The lower panels show plots of single-trial beta weights in T1RT2L and T1LT2R trials, color-coded (red: positive, green: zero, blue: negative). T1-N1 activity can reliably be detected on a single-trial level in both hemispheres. Ticks on the y-axis are every 50 trials. (B) T2-N1 responses. The upper panels show average beta time courses in T1LT2R and T1RT2L trials, separately for SOA 100 (red), SOA 300 (green), and SOA 800 (blue). The upper left panel shows T2-N1 activity in the left hemisphere, the upper right panel shows T2-N1 activity in the right hemisphere. In the left hemisphere, stimulus-locked N1 can be detected at all SOAs (latencies: 272, 472, and 972 msec). In the right hemisphere, stimulus-locked N1 can be detected as well, but the N1 peak at SOA 300 does not reach significance (latencies: 260, 468, and 972 msec). Horizontal bars above the x-axis indicate significant time points (deviation from zero). The lower panels show plots of single-trial beta weights in T1LT2R and T1RT2L trials, color-coded (red: positive, green: zero, blue: negative). T2-N1 activity can reliably be detected on a single-trial level in both hemispheres. Small vertical bars on the x-axis indicate T2 onset at SOA 100, 300, and 800 msec. Ticks on the y-axis are every 50 trials.
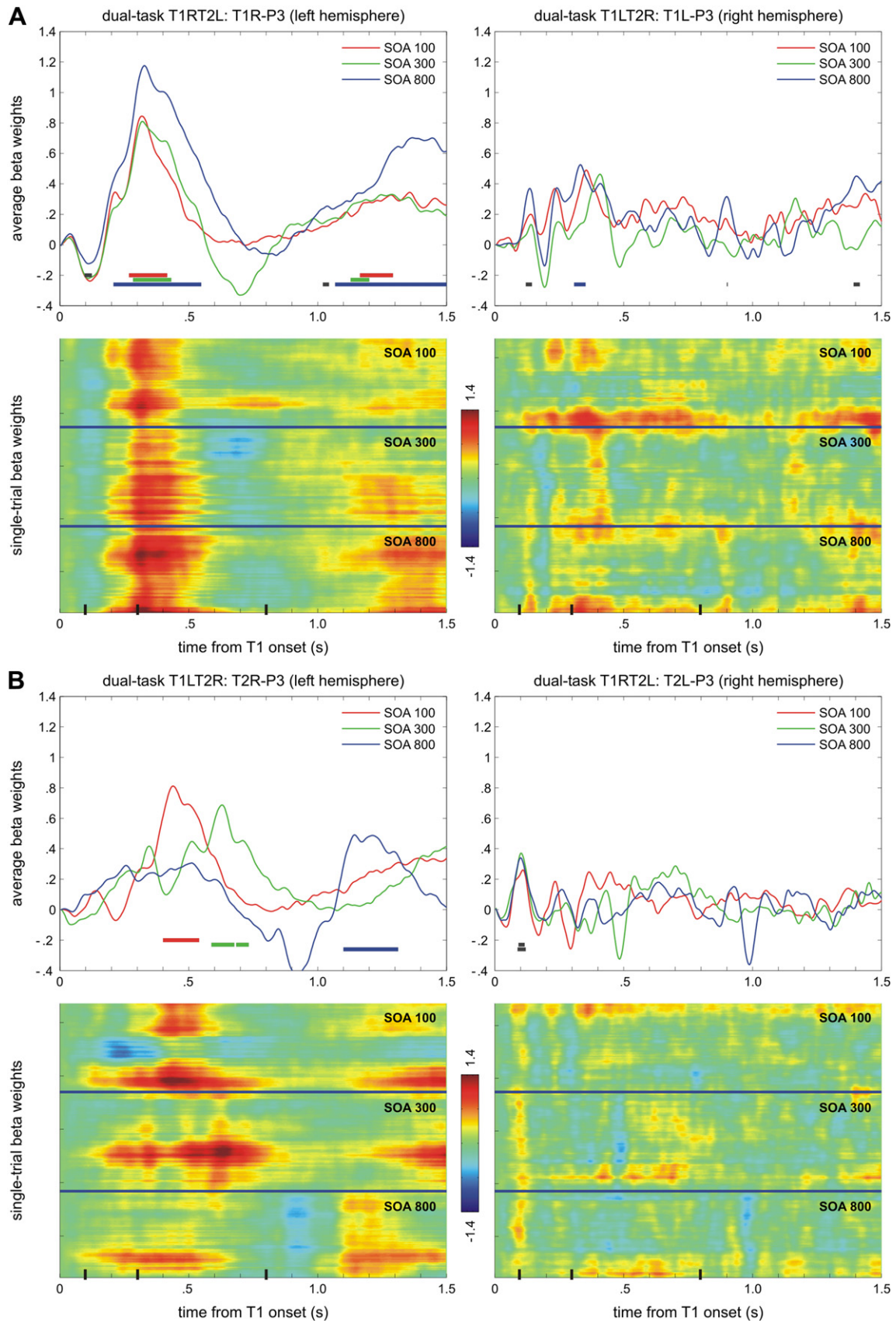
Fig. 8 − Analysis of central ERP components in dual-task trials. (A) T1-P3 responses. The upper panels show average beta time courses in T1RT2L and T1LT2R trials, separately for SOA 100 (red), SOA 300 (green), and SOA 800 (blue). The upper left panel shows T1-P3 activity in the left hemisphere, the upper right panel shows T1-P3 activity in the right hemisphere.

	SOA 100	SOA 300	SOA 800
T1LT2L trials			
RT1	803 ± 262	627 ± 105	600 ± 72
RT1 congruent	795 ± 250	621 ± 110	597 ± 63
RT1 incongruent	811 ± 275	634 ± 100	603 ± 81
RT2	1175 ± 275	860 ± 197	684 ± 172
RT2 congruent	1192 ± 260	852 ± 188	672 ± 183
RT2 incongruent	1158 ± 290	868 ± 209	696 ± 163
Accuracy task 1	89.6%	87.5%	80.2%
Accuracy task 2	78.1%	83.3%	83.3%
r(RT1, RT2)	.71	.36	.01
T1RT2L trials			
RT1	865 ± 270	744 ± 286	660 ± 161
RT1 congruent	810 ± 269	738 ± 301	663 ± 174
RT1 incongruent	920 ± 262	733 ± 274	656 ± 149
RT2	1104 ± 290	822 ± 247	573 ± 112
RT2 congruent	1022 ± 309	827 ± 271	549 ± 116
RT2 incongruent	1185 ± 243	816 ± 222	596 ± 104
Accuracy task 1	92.7%	87.5%	88.5%
Accuracy task 2	90.6%	87.5%	83.3%
r(RT1, RT2)	.80	.81	.26

Fig. 7A (upper panels) shows that, as in the healthy control group, the N1 evoked by the first target (T1-N1) was reliably recovered for all SOAs in T1LT2R and T1RT2L trials, peaking at approximately 168 msec after T1 onset. Positive beta weights for T1-N1 in the left hemisphere were significantly larger than in the right hemisphere ($F_{1,91} = 25.39$, $p < .001$, $\eta^2 = .22$); the main effect "SOA" was not significant ($F < 1$), and we found no significant "hemisphere × SOA" interaction ($F_{2,182} = 1.63$, $p = .198$, $\eta^2 = .02$, $\varepsilon = .99$). T1-N1 betas for RVF targets were preceded by negative betas peaking at approximately 100 msec, which very likely are related to P1 activity (see RVF-N1 betas in T1R trials, Fig. 4C). Lower panels in Fig. 7A, showing single-trial beta weights, confirm that T1-N1 activity could reliably be detected at the expected latencies in both hemispheres on a trial-by-trial basis. Inspection of "raw" averaged ERP amplitudes also revealed smaller T1-N1 components in the right hemisphere, while T1-P1 amplitudes were comparable in both hemispheres (Fig. 3). This result suggests that the finding of smaller N1 betas in the right hemisphere was not simply due to a mismatch between the spatio-temporal templates and the dual-task EEG data.

Fig. 7B (upper panels) illustrates that the N1 evoked by the second target (T2-N1) remained stimulus-locked in dual-task trials as well, as previously reported for normal subjects (Hesselmann et al., 2011; Sigman and Dehaene, 2008). Similar to the T1-N1, the second N1 was significantly larger in the left than in the right hemisphere ($F_{1,91} = 21.82$, $p < .001$, $\eta^2 = .19$), while the main effect "SOA" turned out to be not significant ($F < 1$). The ANOVA yielded a significant "hemisphere × SOA" interaction ($F_{2,182} = 5.12$, $p = .007$, $\eta^2 = .05$, $\varepsilon = .93$), due to the fact that the T2-N1 at SOA 300 was comparably large in the left hemisphere, and small in the right hemisphere. Lower panels in Fig. 7B, showing single-trial beta weights, provide further evidence for the stimulus-locking of the T2-N1, as well as for the amplitude difference between hemispheres. Finally, a comparison between T1-N1 and T2-N1 beta weights revealed no significant difference ($F < 1$).

3.6. EEG results: dual-task (P3)

Fig. 8A (upper panels) shows that, in dual-task trials, significant T1-P3 activity could only be observed in the left hemisphere, peaking at approximately 328 msec, across all SOAs. This finding is confirmed by single-trial beta weights in T1LT2R and T1RT2L trials (Fig. 8A, lower panels). Therefore, we restricted the ANOVA to EEG data from the left hemisphere. T1-P3 activity in the left hemisphere appeared to be largest for SOA 800, yet the main effect "SOA" did not turn out to be significant ($F_{2,184} = 1.75$, $p = .176$, $\eta^2 = .02$, $\varepsilon = .99$). Inspection of "raw" ERP amplitudes in parietal electrodes revealed that, in the patient's right hemisphere, P3-like activity is present only in a number of trials at SOA 100 (data not shown). Thus, the absence of significant T1-P3 beta weights for the right hemisphere cannot be accounted for by a mismatch between the spatio-temporal template and dual-task EEG data. Analysis of ERP responses in more centrally located electrode clusters yielded similar results.

Similar to the T1-P3 findings described above, significant T2-P3 activity could only be observed in the left hemisphere (Fig. 8B, upper panels). This finding is confirmed by single-trial beta weights (Fig. 8B, lower panels). As before, we restricted the ANOVA to data from the left hemisphere. T2-P3 activity was significantly modulated by SOA ($F_{2,182} = 6.80$, $p = .003$, $\eta^2 = .07$, $\varepsilon = .83$); post-hoc t-tests revealed that betas for SOA 800 were smaller than for SOA 100 and for SOA 300 ($p < .001$, $p = .006$; not corrected for multiple comparisons).

In the left hemisphere, P3 can be detected at all SOAs (latency: 328 msec). In the right hemisphere, significant P3 related activity appears to be absent. Horizontal bars above the x-axis indicate significant time points (deviation from zero). The lower panels show plots of single-trial beta weights in T1RT2L and T1LT2R trials, color-coded (red: positive, green: zero, blue: negative). T1-P3 activity can reliably be detected on a single-trial level only in the left hemisphere. Ticks on the y-axis are every 50 trials. (B) T2-P3 responses. The upper panels show average beta time courses in T1LT2R and T1RT2L trials, separately for SOA 100 (red), SOA 300 (green), and SOA 800 (blue). The upper left panel shows T2-P3 activity in the left hemisphere, the upper right panel shows T2-P3 activity in the right hemisphere. In the left hemisphere, P3 can be detected at all SOAs (latencies: 440, 632, and 1144 msec). In the right hemisphere, significant P3 related activity appears to be absent. Horizontal bars above the x-axis indicate significant time points (deviation from zero). The lower panels show plots of single-trial beta weights in T1RT2L and T1LT2R trials, color-coded (red: positive, green: zero, blue: negative). T2-P3 activity can be only identified in the left hemisphere. Small vertical bars on the x-axis indicate T2 onset at SOA 100, 300, and 800 msec. Ticks on the y-axis are every 50 trials.
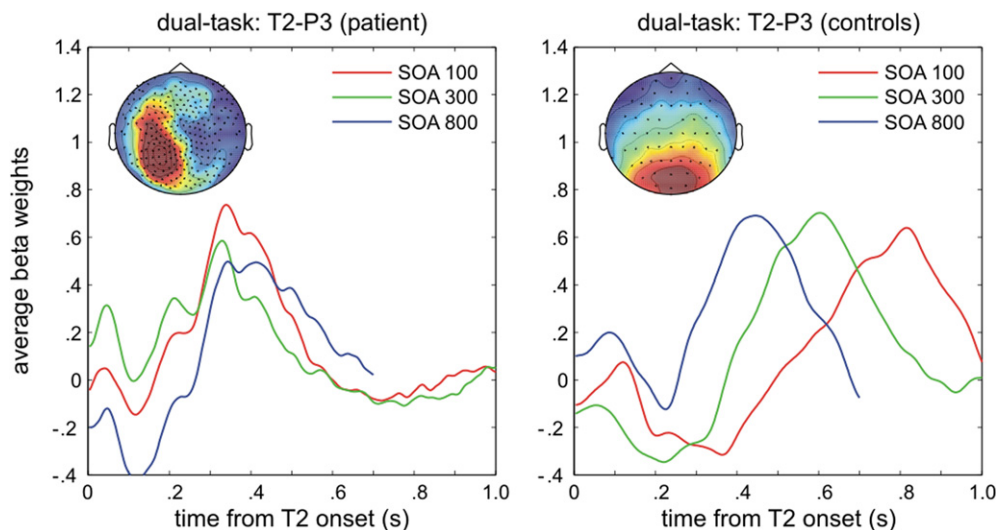
Fig. 9 – Dual-task T2-P3 responses in the patient (left panel) and the control subjects (right panel, N = 12). Shown are the average T2-P3 beta time courses for SOA 100 (red), SOA 300 (green), and SOA 800 (blue) from T2 onset. Topographies represent the RVF-P3 for the patient (latency: 328 msec) and the average of LVF-P3 and RVF-P3 for controls (latency: 380 msec). Missing values for SOA 800 (>.7 sec) are the result of EEG segmentation (−.2–1.5 sec from T1 onset). The offset at T2 onset (0 sec) is due to the fact that the T2-P3 beta weights were baseline corrected with respect to T1 onset. The topographies are 2D representations of the different 3D electrode layouts (patient: 256 electrodes, Pz is the fifth midline channel from the bottom; controls: 62 electrodes, Pz is the third midline channel from the bottom).

Fig. 9 illustrates the significant difference in T2-postponement between patient (left panel) and controls (right panel) by plotting T2-P3 beta weights from T2 onset for all SOAs. Contrary to previous findings in normal subjects (Hesselmann et al., 2011; Sigman and Dehaene, 2008), the patient's T2-P3 showed only minimal latency postponement at short SOAs during the PRP, an observation which was corroborated by inspection of the "raw" averaged ERP amplitudes in parietal electrodes (Fig. 3). For SOA 100, the T2-P3 latency was estimated at 340 msec relative to T2 onset, i.e., with a delay of 12 msec relative to T1-P3 latency in single-task trials. At SOAs 300 and 800, the average T2-P3 peaks were estimated at 332 msec (delay: 4 msec) and 344 msec (delay: 16 msec), respectively. In the healthy controls, the corresponding T2-P3 delays were 280 msec ($t_{11} = 5.90$, $p < .001$), 174 msec ($t_{11} = 3.67$, $p < .005$), and 8 msec ($t_{11} < 1$), and were of comparable magnitude as the behavioral PRP effects [(RT2 minus single-task RT): 299 msec at SOA 100, and 127 msec at SOA 300]. Finally, a direct comparison revealed that beta weights were significantly larger for T1-P3 than T2-P3 in the patient ($F_{1,276} = 10.87$, $p = .001$, $\eta^2 = .04$).

4.   Discussion

In this study, we have probed the brain mechanisms underlying dual-task processing in a patient (AC) with posterior callosal section using a lateralized number-comparison task. Behaviorally, the patient appeared to show a PRP effect superficially similar to that found in the healthy control group, yet with important differences (SOA effect on RT1, RT slopes, and crosstalk). At the neurophysiological level, we were able

to decompose single-task and dual-task ERPs into subcomponents in the patient, and found larger N1 activity in the left than in the right hemisphere and only low-amplitude to nonexistent P3(b) activity in the right hemisphere in dual-task trials. Furthermore, the P3 evoked by RVF targets was "split", showing a distinctly contralateral topography, and was not postponed by the PRP effect, in strong contrast to the significant T2-P3 postponement found in the healthy control group. Each of these points is discussed in turn.

4.1.   PRP and crosstalk effects

The behavioral data revealed that patient AC was able to accurately perform the lateralized number-comparison task, which is in agreement with previous reports of spared smaller–larger magnitude comparison for Arabic numbers in split-brain patients (Colvin et al., 2005; Seymour et al., 1994) and in a patient with posterior callosal lesion (Cohen and Dehaene, 1996). In contrast to the healthy control group, the patient's RTs were modulated by visual field: responses to RVF targets were longer than to LVF targets. An attentional bias toward the left visual hemifield underlying the RT effect seems highly unlikely, given the fact that the amplitudes of the sensory N1 component were significantly larger for RVF than for LVF targets. A left field/right hemisphere advantage for number-comparison tasks has not been reported previously. However, this finding has to be interpreted with caution, since it cannot be ruled out that the damage to the patient's left parietal lobe contributed to this effect.

In agreement with previous reports of robust PRP effects in callosum-sectioned patients (Ivry et al., 1998; Ivry and Hazeltine, 2000; Pashler et al., 1994), patient AC's dual-task

performance showed a lengthening of RT2 and significant RT1-RT2 correlations at short SOAs, which are considered as the hallmarks of the PRP(Pashler, 1994; Pashler and Johnston, 1989). RT1 in T1LT2R trials was modulated by SOA to a larger degree than in the healthy sample, indicating that the patient's right hemisphere was more sensitive than normal to SOA effects; in addition, RT2 slopes observed for patient AC were consistently steeper than in the control group. Analysis of behavioral crosstalk effects in congruent and incongruent trials revealed an effect of target laterality: when the first target was presented on the left (T1LT2R trials), crosstalk was absent; however, when the first target was presented on the right (T1RT2L trials), we found significant crosstalk from T1 to T2 in the RT2 data, which was of comparable magnitude as in the controls, but only marginally significant backward crosstalk. Thus, T2 processing was maximally insensitive to dual-task interference when the second target was presented to the left hemisphere (T1LT2R trials). A similar insensitivity of the left hemisphere to inference has recently been reported in a split-brain patient with callosal anarchic-hand syndrome (Verleger et al., 2011). In a Simon task (Simon, 1969), the patient's (GH) left-hemispheric motor system remained insensitive against interfering motor signals from the right-hemispheric motor system, but not vice versa. Giesbrecht and Kingstone (2004) investigated the behavioral performance of a split-brain patient (JW) in the attentional blink (AB) paradigm, which is closely related to the PRP (Wong, 2002; Jolicœur, 1999; Arnell and Duncan, 2002; Marti et al., 2012).Their study showed that behavioral performance during the AB was more impaired when T2 was presented to the right hemisphere.

It remains unclear to what degree strategical task monitoring might have affected the observed robust dual-task interference in patient AC (Schumacher et al., 2001; Hazeltine et al., 2008). However, the fact that response times to T1 were slowed at short SOAs, considerably more than in normal subjects, suggests that the dual-task slowing effect we observed in the patient may indeed not have the same origin as in normals. In healthy controls, the first task typically unfolds almost without any influence of the presence of a second stimulus at short or long SOA. The fact that patient AC was, paradoxically, enormously slowed by a quasi-simultaneous T2 stimulus in the other hemifield, is compatible with the proposal that task prioritization may pose a specific problem for callosal patients who are trying to follow the instruction of responding first to the stimulus that came first (Hazeltine et al., 2008). According to this argument, the superficial presence of a PRP effect in callosal patients, even seemingly larger than in normals, may in fact hide a considerable degree of parallel processing at the brain level (Hazeltine et al., 2008). Indeed, our ERP data provided direct evidence supporting this idea.

4.2.   ERP decomposition of the PRP effect

In patient AC and in the control group, we found the sensory N1 component to be fully stimulus-locked for T1 and T2, in accordance with earlier ERP studies of the PRP effect (Sigman and Dehaene, 2008; Brisson and Jolicœur, 2007; Hesselmann et al., 2011). Furthermore, we observed no attenuation of the T2-N1 during the PRP. Together, these data provide further

evidence that perceptual processing occurs in parallel for T1 and T2 in our lateralized dual-task paradigm.

Analysis of P3 responses revealed a strictly contralateral T1-P3 in the patient, i.e., a subdivision or "splitting" into LVF-P3 for LVF targets and RVF-P3 for RVF targets, unlike in normal subjects where we found a single parietal P3 in the same task (Hesselmann et al., 2011). Analysis of the moment-to-moment correlations between ERP topographies in single-task T1L and T1R trials corroborated this finding: while topographies converged toward a shared pattern at the time of the P3 in controls, the topographies remained highly dissimilar until a much later time period in the patient (~600 msec). This finding extends a previous report of ERP asymmetry in the same patient, which showed that LVF and RVF targets evoke highly different ERPs that remain largely contralateral for a long period, between approximately 200 and 620 msec after target onset (Cohen et al., 2000). The observed late convergence toward a shared topography was probably mediated by intact anterior commissural connections in patient AC, which have been implicated in the transfer of stimulus-related semantic activation in partial split-brain patients (Sidtis et al., 1981). Our finding appears to be in good agreement with a conceptualization of P3 in which there are multiple cognitive processes and neural generators underlying its generation (Johnson, 1993, 1986). This model has received confirmatory evidence from intracranial recordings and EEG-fMRI studies showing a highly distributed set of activated areas including hippocampus and temporal, parietal, and frontal association cortices (Halgren et al., 1998; Mantini et al., 2009).

In the single-task condition, the LVF-P3 was absent in most trials but of comparable amplitude to the RVF-P3 when being present. In dual-task trials, this difference was even more expressed, and LVF-P3 was virtually absent for T1 and T2. This striking hemisphere difference cannot simply be accounted for by the patient's neurological status, since his right hemisphere (supposedly the neural origin of the LVF-P3) was intact. Speculatively, P3 attenuation in the right hemisphere might be directly related to our finding of maximal behavioral dual-task interference when the second target is presented to the LVF. However, LVF-P3 was also virtually absent for T1 in dual-task trials. Alternatively, our findings could suggest that the P3, which reflects access to a central stage of distributed processing associated with conscious report (Sergent et al., 2005; Del Cul et al., 2007), might arise predominantly from left-hemispheric networks when inter-hemispheric transfer is fully or partly disrupted and the hemispheres are "isolated". At this stage, this possibility remains speculative, and a conclusion on this point will have to await further research. P3 asymmetries have previously been reported for split-brain (Proverbio et al., 1994; Verleger et al., 2011; Kutas et al., 1990; Satomi et al., 1995) and callosal agenesis patients (Bayard et al., 2004), but the emerging picture is not yet conclusive. In normal subjects, ERP studies have suggested that corpus callosal size (as indexed by handedness) might be related to P3 amplitude and latency (Hoffman and Polich, 1999).

Similarly to the N1, both amplitude and latency of the T1-P3 remained unaffected by SOA, in the patient and in healthy controls. Latency of the T2-P3, however, showed significant PRP-related postponement in controls (Hesselmann et al., 2011), but remained remarkably time-

locked to T2 onset in patient AC. This observed absence of T2-P3 postponement suggests greater parallel processing in patient AC, afforded by the partial disconnection of the two hemispheres. It is compatible with the existence of a temporary period during which two distinct states of global intra-hemispheric communication ("global workspaces") coexist and permit partially parallel decision making, unlike normal subjects in whom the presence of a global bi-hemispheric state enforces serial processing of dual tasks (Hesselmann et al., 2011; Dehaene and Naccache, 2001). Previous split-brain studies have reported various cognitive processes that can be performed in parallel by the left and right hemispheres after commissurotomy, e.g., visual search for conjunction targets in bilateral arrays (Luck et al., 1989, 1994).

The possibility of two separate global neuronal workspaces in patient AC – strictly limited to the first few hundred milliseconds of stimulus processing – raises the question of the quality of his subjective visual awareness during that time period (Dehaene and Changeux, 2011). Conceivably, his conscious awareness of the two targets might be delayed by ∼600 msec, i.e., until a shared ERP topography on the scalp indicated a successful interaction between higher-level post-sensory decision processes in each hemisphere (Sidtis et al., 1981). This hypothesis could be directly tested using measures of quantified introspection (Marti et al., 2010; Corallo et al., 2008). In normal subjects, related delays of temporal selection, which diminish the conscious report of a target stimulus, have already been shown for the AB (Vul et al., 2008). More speculatively, there could exist a brief period with two separate states of visual awareness in patient AC, limited to the time between the completion of sensory processing and the beginning of higher-level inter-hemispheric communication. If, however, the P3 component is taken as an indicator of conscious access (Del Cul et al., 2007; Gaillard et al., 2009; Sergent et al., 2005), then its absence over the right hemisphere for LVF targets, specifically during dual-task processing, may indicate a single episode of conscious access restricted to the RVF target (whether presented first or second), with much delayed or reduced conscious access to the LVF target. Again, these hypotheses could be evaluated through quantified introspection (Marti et al., 2010; Corallo et al., 2008).

4.3. Concluding remarks

This study is the first to investigate PRP effects in a patient with posterior callosal section using high-density EEG. We have shown that ERP signatures of dual-task limitations are affected when the two hemispheres are (partially) disconnected. The neurophysiological evidence suggests a considerable degree of parallel processing, even at the level of central stages that are normally postponed and unfold strictly serially in normal subjects. Follow-up studies could compare patient AC's behavioral and ERP results to that from surgical split-brain patients, and include single-trial measures of both P3 amplitude and latency to further explore conscious access in isolated hemispheres (Dehaene and Changeux, 2011). Recent advances in neuroimaging techniques also open up a fascinating opportunity to relate PRP effects in lateralized tasks to individual measures of inter-hemispheric communication in normal subjects (Doron and Gazzaniga, 2008; Genc et al., 2011).

Supplementary material

Supplementary data associated with this article can be found in the online version, at doi:10.1016/j.cortex.2012.03.014.

REFERENCES

Arnell KM and Duncan J. Separate and shared sources of dual-task costs in stimulus identification and response selection. *Cognitive Psychology*, 44: 105–147, 2002.

Arnell KM, Helion AM, Hurdelbrink JA, and Pasieka B. Dissociating sources of dual-task interference using human electrophysiology. *Psychonomic Bulletin and Review*, 11(1): 77–83, 2004.

Banich MT. The missing link: The role of interhemispheric interaction in attentional processing. *Brain and Cognition*, 36(2): 128–157, 1998.

Bayard S, Gosselin N, Robert M, and Lassonde M. Inter- and intrahemispheric processing of visual event-related potentials in the absence of the corpus callosum. *Journal of Cognitive Neuroscience*, 16(3): 401–414, 2004.

Bell AJ and Sejnowski TJ. An information maximisation approach to blind separation and blind deconvolution. *Neural Computation*, 7: 1129–1159, 1995.

Blair RC and Karniski W. An alternative method for significance testing of waveform difference potentials. *Psychophysiology*, 30(5): 518–524, 1993.

Brisson B and Jolicœur P. Electrophysiological evidence of central interference in the control of visuospatial attention. *Psychonomic Bulletin and Review*, 14(1): 126–132, 2007.

Cohen J. *Statistical Power Analysis for the Behavior Sciences*. 2nd ed. Hillsdale, NJ: Erlbaum, 1988.

Cohen L and Dehaene S. Cerebral networks for number processing: Evidence from a case of posterior callosal lesion. *Neurocase*, 2: 155–174, 1996.

Cohen L, Dehaene S, Naccache L, Lehericy S, Dehaene-Lambertz G, Henaff MA, et al. The visual word form area: Spatial and temporal characterization of an initial stage of reading in normal subjects and posterior split-brain patients. *Brain*, 123(2): 291–307, 2000.

Colvin MK, Funnell MG, and Gazzaniga MS. Numerical processing in the two hemispheres: Studies of a split-brain patient. *Brain and Cognition*, 57(1): 43–52, 2005.

Corallo G, Sackur J, Dehaene S, and Sigman M. Limits on introspection: Distorted subjective time during the dual-task bottleneck. *Psychological Science*, 19(11): 1110–1117, 2008.

Crawford JR and Howell DC. Comparing an individual's test score against norms derived from small samples. *The Clinical Neuropsychologist*, 12(4): 482–486, 1998.

De Jong R. Multiple bottlenecks in overlapping task performance. *Journal of Experimental Psychology: Human Perception and Performance*, 19(5): 965–980, 1993.

Dehaene S and Changeux JP. Experimental and theoretical approaches to conscious processing. *Neuron*, 70(2): 200–227, 2011.

Dehaene S and Naccache L. Towards a cognitive neuroscience of consciousness: Basic evidence and a workspace framework. *Cognition*, 79(1–2): 1–37, 2001.

Dehaene S, Naccache L, Le Clec'H G, Koechlin E, Mueller M, Dehaene-Lambertz G, et al. Imaging unconscious semantic priming. *Nature*, 395(6702): 597–600, 1998.

Del Cul A, Baillet S, and Dehaene S. Brain dynamics underlying the nonlinear threshold for access to consciousness. *PLoS Biology*, 5(10): 1–16, 2007.

Dell'Acqua R, Jolicœur P, Vespignani F, and Toffanin P. Central processing overlap modulates P3 latency. *Experimental Brain Research*, 165(1): 54–68, 2005.

Delorme A and Makeig S. EEGlab: An open source toolbox for analysis of single-trial EEG dynamics. *Journal of Neuroscience Methods*, 134(1): 9–21, 2004.

Donchin E. Surprise!.Surprise? *Psychophysiology*, 18(5): 493–513, 1981.

Donchin E and Coles MG. Is the P300 component a manifestation of context updating? *Behavioral and Brain Sciences*, 11(3): 357–374, 1988.

Doron KW and Gazzaniga MS. Neuroimaging techniques offer new perspectives on callosal transfer and interhemispheric communication. *Cortex*, 44(8): 1023–1029, 2008.

Frak V, Paulignan Y, Jeannerod M, Michel F, and Cohen H. Prehension movements in a patient (AC) with posterior parietal cortex damage and posterior callosal section. *Brain and Cognition*, 60(1): 43–48, 2006.

Franz EA, Eliassen JC, Ivry RB, and Gazzaniga MS. Dissociation of spatial and temporal coupling in the bimanual movements of callosotomy patients. *Psychological Science*, 7(5): 306–310, 1996.

Gaillard R, Dehaene S, Adam C, Clemenceau S, Hasboun D, Baulac M, et al. Converging intracranial markers of conscious access. *PLoS Biology*, 7: e61, 2009.

Gazzaniga MS. Principles of human brain organization derived from split-brain studies. *Neuron*, 14(2): 217–228, 1995.

Gazzaniga MS. Forty-five years of split-brain research and still going strong. *Nature Reviews Neuroscience*, 6(8): 653–659, 2005.

Genc E, Bergmann J, Singer W, and Kohler A. Interhemispheric connections shape subjective experience of bistable motion. *Current Biology*, 21(17): 1494–1499, 2011.

Giesbrecht B and Kingstone A. Right hemisphere involvement in the attentional blink: Evidence from a split-brain patient. *Brain and Cognition*, 55(2): 303–306, 2004.

Greenhouse SW and Geisser S. On methods in the analysis of profile data. *Psychometrika*, 24(2): 95–112, 1959.

Groppe DM, Urbach TP, and Kutas M. Mass univariate analysis of event-related brain potentials/fields I: A critical tutorial review. *Psychophysiology*, 48(12): 1711–1725, 2011.

Halgren E, Marinkovic K, and Chauvel P. Generators of the late cognitive potentials in auditory and visual oddball tasks. *Electroencephalography and Clinical Neurophysiology*, 106(2): 156–164, 1998.

Hazeltine E, Weinstein A, and Ivry RB. Parallel response selection after callosotomy. *Journal of Cognitive Neuroscience*, 20(3): 526–540, 2008.

Hesselmann G, Flandin G, and Dehaene S. Probing the cortical network underlying the psychological refractory period: A combined EEG-fMRI study. *NeuroImage*, 56(3): 1608–1621, 2011.

Hofer S and Frahm J. Topography of the human corpus callosum revisited – Comprehensive fiber tractography using diffusion tensor magnetic resonance imaging. *NeuroImage*, 32(3): 989–994, 2006.

Hoffman LD and Polich J. P300, handedness, and corpus callosal size: Gender, modality, and task. *International Journal of Psychophysiology*, 31(2): 163–174, 1999.

Holtzman JD and Gazzaniga MS. Dual task interactions due exclusively to limits in processing resources. *Science*, 218(4579): 1325–1327, 1982.

Intriligator J, Henaff MA, and Michel F. Able to name, unable to compare: The visual abilities of a posterior split-brain patient. *NeuroReport*, 11(12): 2639–2642, 2000.

Isreal JB, Chesney GL, Wickens CD, and Donchin E. P300 and tracking difficulty: Evidence for multiple resources in dual-task performance. *Psychophysiology*, 17(3): 259–273, 1980.

Ivry R and Hazeltine E. Task switching in a callosotomy patient and normal participants: Evidence for response-related sources of interference. In Monsell R and Driver J (Eds) Attention and Performance XVIII. Cambridge, MA: MIT Press, 2000: 401–423.

Ivry RB, Franz EA, Kingstone A, and Johnston JC. The psychological refractory period effect following callosotomy: Uncoupling of lateralized response codes. *Journal of Experimental Psychology: Human Perception and Performance*, 24(2): 463–480, 1998.

Johannes S, Münte TF, Heinze HJ, and Mangun GR. Luminance and spatial attention effects on early visual processing. *Cognitive Brain Research*, 2(3): 189–205, 1995.

Johnson Jr R. A triarchic model of P300 amplitude. *Psychophysiology*, 23(4): 367–384, 1986.

Johnson Jr R. On the neural generators of the P300 component of the event-related potential. *Psychophysiology*, 30(1): 90–97, 1993.

Jolicœur P. Concurrent response-selection demands modulate the attentional blink. *Journal of Experimental Psychology: Human Perception and Performance*, 25(4): 1097–1113, 1999.

Kok A. On the utility of P3 amplitude as a measure of processing capacity. *Psychophysiology*, 38(3): 557–577, 2001.

Kutas M, Hillyard SA, Volpe BT, and Gazzaniga MS. Late positive event-related potentials after commissural sections in humans. *Journal of Cognitive Neuroscience*, 2(3): 258–271, 1990.

Lehmann D and Skrandies W. Reference-free identification of components of checkerboard-evoked multichannel potential fields. *Electroencephalography and Clinical Neurophysiology*, 48(6): 609–621, 1980.

Logan GD and Delheimer JA. Parallel memory retrieval in dual-task situations: II. Episodic memory. *Journal of Experimental Psychology: Learning, Memory and Cognition*, 27(3): 668–685, 2001.

Logan GD and Schulkind MD. Parallel memory retrieval in dual-task situations: I. Semantic memory. *Journal of Experimental Psychology: Human Perception and Performance*, 26(3): 1072–1090, 2000.

Luck SJ. Sources of dual-task interference: Evidence from human electrophysiology. *Psychological Science*, 9(3): 223–227, 1998.

Luck SJ, Hillyard SA, Mangun GR, and Gazzaniga MS. Independent hemispheric attentional systems mediate visual search in split-brain patients. *Nature*, 342(6249): 543–545, 1989.

Luck SJ, Hillyard SA, Mangun GR, and Gazzaniga MS. Independent attentional scanning in the separated hemispheres of split-brain patients. *Journal of Cognitive Neuroscience*, 6(1): 84–91, 1994.

Mantini D, Corbetta M, Perrucci MG, Romani GL, and Del Gratta C. Large-scale brain networks account for sustained and transient activity during target detection. *NeuroImage*, 44(1): 265–274, 2009.

Marois R and Ivanoff J. Capacity limits of information processing in the brain. *Trends in Cognitive Sciences*, 9(6): 296–305, 2005.

Marti S, Sackur J, Sigman M, and Dehaene S. Mapping introspection's blind spot: Reconstruction of dual-task phenomenology using quantified introspection. *Cognition*, 115(2): 303—313, 2010.

Marti S, Sigman M, and Dehaene S. A shared cortical bottleneck underlying attentional blink and psychological refractory period. *NeuroImage*, 59(3): 2883—2898, 2012.

Michel F, Henaff MA, and Intriligator J. Two different readers in the same brain after a posterior callosal lesion. *NeuroReport*, 7(3): 786—788, 1996.

Miller J. Backward crosstalk effects in psychological refractory period paradigms: Effects of second-task response types on first-task response latencies. *Psychological Research*, 70(6): 484—493, 2006.

Mognon A, Jovicich J, Bruzzone L, and Buiatti M. ADJUST: An automatic EEG artifact detector based on the joint use of spatial and temporal features. *Psychophysiology*, 48(2): 229—240, 2011.

Naccache L and Dehaene S. Unconscious semantic priming extends to novel unseen stimuli. *Cognition*, 80(3): 215—229, 2001.

Navon D and Miller J. Queuing or sharing? A critical evaluation of the single-bottleneck notion. *Cognitive Psychology*, 44(3): 193—251, 2002.

Oostenveld R, Fries P, Maris E, Schoffelen JM. FieldTrip: Open source software for advanced analysis of MEG, EEG, and invasive electrophysiological data. *Computational Intelligence and Neuroscience*, 1—9, 2011. doi:10.1155/2011/156869.

Pashler H. Dual-task interference in simple tasks: Data and theory. *Psychological Bulletin*, 116(2): 220—244, 1994.

Pashler H. *The Psychology of Attention*. Cambridge: MA MIT Press, 1998.

Pashler H and Johnston JC. Interference between temporally overlapping tasks: Chronometric evidence for central postponement with or without response grouping. *Quarterly Journal of Experimental Psychology*, 41A(1): 19—45, 1989.

Pashler H, Luck SJ, Hillyard SA, Mangun GR, O'Brien S, and Gazzaniga MS. Sequential operation of disconnected cerebral hemispheres in split-brain patients. *NeuroReport*, 5(17): 2381—2384, 1994.

Picton TW. The P300 wave of the human event-related potential. *Journal of Clinical Neurophysiology*, 9(4): 456—479, 1992.

Proverbio AM, Zani A, Gazzaniga MS, and Mangun GR. ERP and RT signs of a rightward bias for spatial orienting in a split-brain patient. *NeuroReport*, 5(18): 2457—2461, 1994.

Sackur J, Naccache L, Pradat-Diehl P, Azouvi P, Mazevet D, Katz R, et al. Semantic processing of neglected numbers. *Cortex*, 44(6): 673—682, 2008.

Satomi K, Horai T, Kinoshita Y, and Wakazono A. Hemispheric asymmetry of event-related potentials in a patient with callosal disconnection syndrome: A comparison of auditory, visual and somatosensory modalities. *Electroencephalography and Clinical Neurophysiology*, 94(6): 440—449, 1995.

Scalf PE, Banich MT, Kramer AF, Narechania K, and Simon CD. Double take: Parallel processing by the cerebral hemispheres reduces attentional blink. *Journal of Experimental Psychology: Human Perception and Performance*, 33(2): 298—329, 2007.

Schumacher EH, Seymour TL, Glass JM, Fencsik DE, Lauber EJ, Kieras DE, et al. Virtually perfect time sharing in dual-task performance: Uncorking the central cognitive bottleneck. *Psychological Science*, 12(2): 101—108, 2001.

Sergent C, Baillet S, and Dehaene S. Timing of the brain events underlying access to consciousness during the attentional blink. *Nature Neuroscience*, 8(10): 1391—1400, 2005.

Seymour SE, Reuter-Lorenz PA, and Gazzaniga MS. The disconnection syndrome. Basic findings reaffirmed. *Brain*, 117(1): 105—115, 1994.

Sidtis JJ, Volpe BT, Holtzman JD, Wilson DH, and Gazzaniga MS. Cognitive interaction after staged callosal section: Evidence for transfer of semantic activation. *Science*, 212(4492): 344—346, 1981.

Sigman M and Dehaene S. Parsing a cognitive task: A characterization of the mind's bottleneck. *PLoS Biology*, 3(2): e37, 2005.

Sigman M and Dehaene S. Brain mechanisms of serial and parallel processing during dual-task performance. *Journal of Neuroscience*, 28(30): 7585—7598, 2008.

Simon JR. Reactions toward the source of stimulation. *Journal of Experimental Psychology*, 81(1): 174—176, 1969.

Telford CW. The refractory phase of voluntary and associative responses. *Journal of Experimental Psychology*, 14(1): 1—36, 1931.

Todman JB and Dugard P. *Single-case and Small-n Experiments Designs*. New York: Lawrence Erlbaum Associates, 2001.

Tombu M and Jolicœur P. A central capacity sharing model of dual-task performance. *Journal of Experimental Psychology: Human Perception and Performance*, 29(1): 3—18, 2003.

Verleger R, Binkofski F, Friedrich M, Sedlmeier P, and Kömpf D. Anarchic-hand syndrome: ERP reflections of lost control over the right hemisphere. *Brain and Cognition*, 77(1): 138—150, 2011.

Verleger R, Jaśkowski P, and Wascher E. Evidence for an integrative role of P3b in linking reaction to perception. *Journal of Psychophysiology*, 19(3): 165—181, 2005.

Vul E, Nieuwenstein M, and Kanwisher N. Temporal selection is suppressed, delayed, and diffused during the attentional blink. *Psychological Science*, 19(1): 55—61, 2008.

Welford AT. The 'psychological refractory period' and the timing of high-speed performance — a review and a theory. *British Journal of Psychology*, 43(1): 2—19, 1952.

Wong KFE. The relationship between attentional blink and psychological refractory period. *Journal of Experimental Psychology: Human Perception and Performance*, 28(1): 54—71, 2002.